RSC Advances

ROYAL SOCIETY OF CHEMISTRY

www.rsc.org/advances

Journal Name

COMMUNICATION

Disorder Engineering of Exotic Electronic 2D TiO_2 Nanosheets for Enhanced Photocatalytic Performance†

Received 00th January 20xx,
Accepted 00th January 20xx

DOI: 10.1039/x0xx00000x

www.rsc.org/

Bo Yan, Pengshang Zhou, Qun Xu*, Xiaofang Zhou, Dongdong Xu, Jianhua Zhu

We successfully prepared the exotic electronic 2D TiO_2 nanosheets and then pursued disorder engineering on it to obtain the black TiO_2 nanosheets. The structure changes induced by disorder engineering were carefully investigated. And the salient properties of the black TiO_2 nanosheets have been evidenced by the enhanced photocurrent and H_2 evolution properties.

As a cheap, efficient, and stable photocatalysts, titanium dioxide (TiO_2) has drawn dense interest owing to its wide applications in solar cells, solar-driven hydrogen production, photocatalytic degradation of dyes and so forth.[1-3] Because the band gap energy of anatase is 3.2 eV that limits its photocatalytic activity in ultraviolet range, great efforts have been dedicated to extend the light absorption of TiO_2 into the visible range of the spectrum and allow more efficient use of solar light.[4] Recently, fabrication of "black" TiO_2 as the breakthrough approach reported by Chen et al., has attracted great attention owing to its high-efficiency enhanced photocatalytic properties.[5] It is suggested that the hydrogenated TiO_2 boost the harvesting solar light impressively by introducing disorder on the surface.[6-7]

Compared with bulk TiO_2 materials, the ultrathin TiO_2 nanosheets own extremely high percentage of surfaces (nearly 100 %), exotic electronic properties and the significant quantum confinement effect in the thinnest dimension,[8] so hydrogenation of them are very necessary. Theoretically, the ultrathin 2D TiO_2 nanosheets are more prone to being hydrogenated, because Ti atoms are on the exposed surface possessing higher electron densities.[9-11] From the point view of application, the quantum confinement effects and the big specific surface area of ultrathin nanosheets are also expected to improve the photocatalytic properties.[12] So exploring hydrogenation of 2D TiO_2 nanosheets to obtain strong and stable photocatalyst as well as investigating the synergistic effect of structure and electron, is an important and attractive research topic.[13]

Fig. 1 schematizes the fabrication of ultrathin black TiO_2 nanosheets. First, the raw-TiO_2 nanosheets were prepared by using P123 as surfactant together with ethylene glycol (EG) as co-surfactant in ethanol solvent. The surfactant and co-surfactant formed inverse lamellar micelles, and the hydrated inorganic oligomers were confined inside it. Then solvothermal treatment was carried out to form crystallized 2D nanosheets.[9] After being washed and dried, the raw-TiO_2 nanosheets were annealed at 400 °C for 1 h to improve the crystallinity. Second, the annealed TiO_2 nanosheets were mixed with $NaBH_4$ powder by grinding thoroughly and heated up to 220-300 °C for 20 minutes under N_2 atmosphere. Then the hydrogenated TiO_2 nanosheets were obtained. As shown in Fig. S1, the color of TiO_2 nanosheets changed from light yellow to dark along with the rising experimental temperature, which implies the enhancement of light adsorption and the potential high-efficiency utilization of sunlight. It is worthwhile to address that, compared with other reports,[13-14] the hydrogenation temperatures in this work are much lower, which indicates that TiO_2 nanosheets are easier to be hydrogenated than bulk TiO_2 materials.

The highly exposed surface of TiO_2 nanosheets can be observed from Fig. S2. The thickness of the ultrathin TiO_2

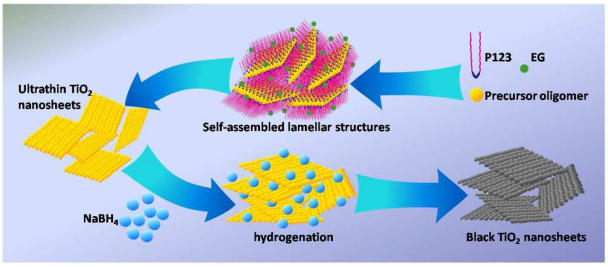

Fig. 1. Schematic synthesis process of the ultrathin black TiO_2 nanosheetts.

[a] College of Materials Science and Engineering, Zhengzhou University, Zhengzhou 450052 (China), E-mail: qunxu@zzu.edu.cn.

† We are grateful for the National Natural Science Foundation of China (Nos. 51173170, 21101141), the financial support from the Innovation Talents Award of Henan Province (114200510019) and the Key program of science and technology (121PZDGG213) from Zhengzhou Bureau of science and technology.
Electronic Supplementary Information (ESI) available: [Detailed experiments and characterization, TEM, XRD and etc.]. See DOI: 10.1039/x0xx00000x

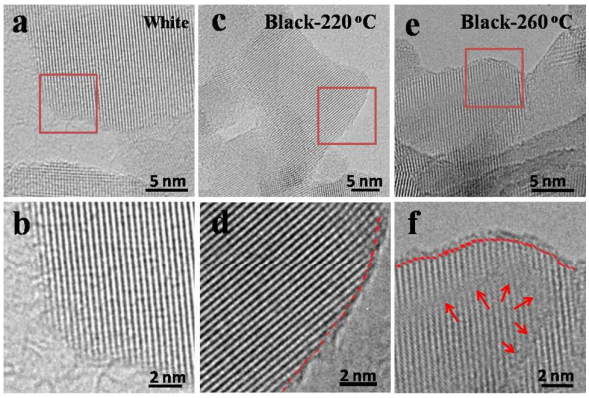

Fig. 2. HRTEM images of the white and black TiO_2 nanosheets that are hydrogenated at different temperatures (a,b: white; c,d: black-220 °C; e,f: black-260 °C; b, d, f correspond with the red box in a, c, e).

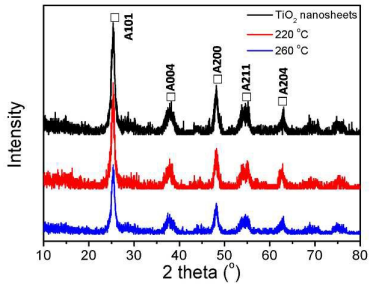

Fig. 3. The XRD patterns of the white and black TiO_2 nanosheets (the white TiO_2 nanosheets were annealed in air; the black was hydrogenated at 220 and 260 °C).

nanosheets is less than 2 nm by observing the edge configuration. The changing process of crystal structure during the hydrogenation can be observed from Fig. 2. Fig. 2a and b are the images of white TiO_2 nanosheets. The clear lattice fringes demonstrate its high crystallization. Fig. 2c and d are the images of samples hydrogenated at 220 °C. It can be found the disordered range began to appear as shown with the dotted line. When the hydrogenation temperature was increased to 260 °C, the surfaces of TiO_2 nanosheets became more disordered, and the disordered outer layer around the crystalline range was about 0.5 nm in thickness shown in Fig. 2e and f, and even to reach 1.0 nm that is shown in Fig. S3f. When the hydrogenation temperature was further raised up to 300 °C, it can be observed that the crystal structures were totally disrupted and their characterization is presented in Fig. S3g-i. So it can be judged that the hydrogenation firstly occurred on the edges of nanosheets because of its great chemical activity,[15] and then gradually with the rising of hydrogenation temperatures, the hydrogenation can occur on the inner surface subsequently. After hydrogenation, the TiO_2 nanosheets maintained the big specific surface area (black-260 °C: 179.6 m^2 g^{-1}, Fig. S4), which also suggested the high exposed surface and the morphology of ultrathin nanosheets.

To reveal the variation of the crystal structure, the as-prepared TiO_2 nanosheets were characterized by X-ray diffraction (XRD). The XRD diffraction indicates that the raw-TiO_2 nanosheets have a phase of TiO_2-B (Fig. S5).[16a] After being annealed, most of the TiO_2 nanosheets turned to be anatase (Fig. 3). The strong XRD diffraction peaks suggest that the TiO_2

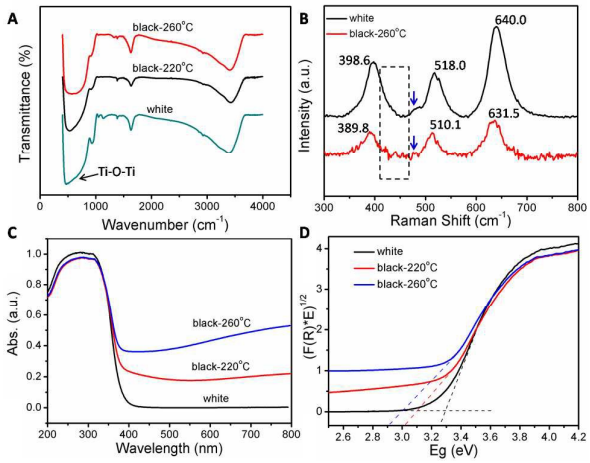

Fig. 4. (A) FTIR spectra of different TiO_2 nanosheets samples. (B) Raman spectra of white and black TiO_2 nanosheets (260 °C). (C) UV–Vis diffuse reflectance absorption (DRS) spectrum of samples. (D) A plot transformed according to the Kubelka-Munk function versus energy of light.

nanosheets were highly crystallized. Along with the raising of hydrogenation temperature, the peaks of samples became weaker. However, the TiO_2 nanosheets hydrogenated at 220 and 260 °C can still present strong XRD peaks (Fig. 3). The occurrence of crystalline lattice deformation and the final disorder played a vital role in the decrease of the XRD peakes.[16b] The disorder appearing at lower hydrogenated temperature also indicates that the 2D TiO_2 nanosheets are much easier to be reduced than bulk materials.

Fourier transform infrared (FTIR) spectra are performed to study the chemical structure of samples, as shown in Fig. 4A. All of samples show strong absorption around 3400 cm^{-1}, 1630 cm^{-1} and 500 cm^{-1}, which are assigned to O-H stretching vibrations of surface hydroxyl groups, H-O-H bending vibrations of physically adsorbed water and Ti–O–Ti stretching vibration of the interconnected octahedral [TiO_6], respectively.[17] As a spectroscopic technique to measure molecular vibrations, Raman spectroscopy is used to examine the chemical structures of the samples. Before hydrogenation, the ultrathin TiO_2 nanosheets not only exhibit E_g modes (640.0 cm^{-1}), B_{1g} mode (398.6 cm^{-1}) and A_{1g} mode (518.0 cm^{-1})(assigned to the anatase), but also appear a new peak between 450-500 cm^{-1} (as the blue arrow indicates) that cannot be ascribed to other phases (rutile and brookite) (Fig. 4B),[18] so it confirmed the different surface chemical states of the ultrathin TiO_2 nanosheets. After hydrogenation, the peak assigned by blue arrow shifted to lower wavenumber. And the typical Raman peaks of TiO_2 undergo a red shift with a wavenumber of about 8 cm^{-1}(E_g= 631.5 cm^{-1}, A_{1g}= 510.1 cm^{-1}, B_{1g}= 389.8 cm^{-1}) as well as the width and height of peaks becomes broader and lower. Besides these modes, an additional active mode ranging from 400 cm^{-1} to 500 cm^{-1} is observed in the black TiO_2 nanosheets (as shown in the dotted box), which cannot be attributed to any phases of TiO_2. A possible explanation is that the hydrogenation of TiO_2 nanosheets can break down the Raman selection rules and

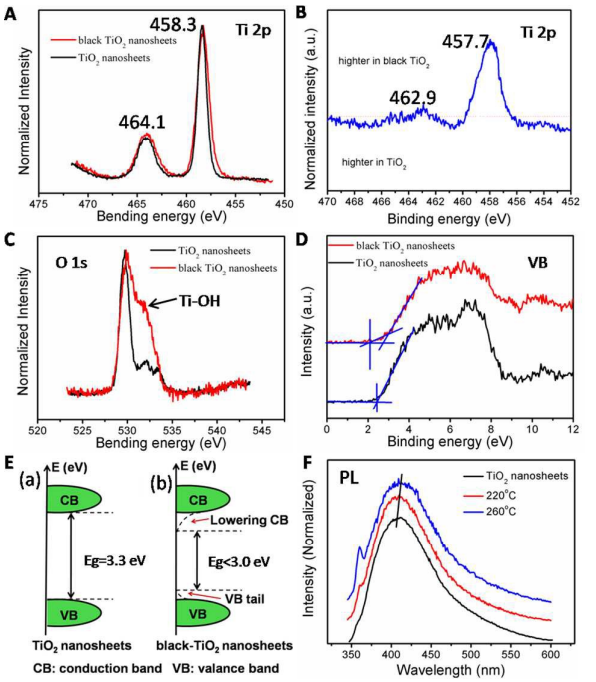

Fig. 5. (A) Ti 2p XPS spectra of the samples. (B) The spectrum of the difference by subtracting the normalized Ti 2p spectra of the black with white TiO_2 nanosheets. (C) O 1s XPS spectra of the white and black samples. (D) XPS valence band spectra of the samples. Blue lines highlight the linear extrapolation of the curves. (E) Schematic of band structures based on the experimental data from UV–vis spectroscopy, and XPS analysis: (a) white TiO_2 nanosheets and (b) black TiO_2 nanosheets. (F) Photoluminescence of samples using 325 nm excitation.

further generate a new active mode by lowering the geometric symmetries of TiO_2.[7b,19]

Compared with the white nanosheets, the hydrogenated samples significantly enhance the absorption of visible light. Fig. 4C indicates the absorption of visible light is promoted along with the increase of the hydrogenated temperature. Moreover, the absorption of black TiO_2 nanosheets in the region of ultraviolet reduces slightly, which can be explained by the structure changes. Considering TiO_2 is an indirect semiconductor, a plot of $(F(R)E)^{1/2}$ versus the energy of absorbed light can be converted according the Kubelka-Munk function from the UV–Vis DRS spectrum,[20] which is expressed in Fig. 4D. The band gap energy of white ultrathin TiO_2 nanosheets estimated from the intercept of the tangent to the plot is larger than 3.3 eV (3.2 eV for bulk TiO_2), which shows a blue shift compared with the bulk materials, demonstrating the quantum confinement effect in the thinnest dimension. After hydrogenation, its band gaps decreased to about 2.9 and 3.1 eV. The reduction of band gaps and the radical changes of visible light absorption are ascribed to the increase of oxygen vacancy and Ti^{3+} concentration through hydrogenation.[5]

X-ray photoelectron spectroscopy (XPS) studies were performed to investigate the chemical binding and valence band position of the samples.[17] Compared with other stoichiometric bulk crystals,[21-22] the white ultrathin TiO_2 nanosheets have a shift to lower binding energy (more than 1 eV, Table S1) of the core level of Ti 2p, which suggests its exotic electronic properties. It was reported that the lower binding energy for surface atoms is the result of electron gain (reduction) of Ti atoms from surrounding oxygen atoms,[9] which indicates the different bonding environments and the easier hydrogenation of TiO_2 nanosheets. And it is in line with the low hydrogenation temperature of ultrathin TiO_2 nanosheets.

Fig. 5A presents the normalized Ti 2p core level XPS spectra of TiO_2 nanosheets before and after hydrogenation. The characteristic peaks of Ti $2p_{1/2}$ and Ti $2p_{3/2}$ peaks of Ti^{4+} center at ~464.1 and ~458.3 eV for both samples.[5,23] The peaks of the black sample show a slight negative shift in binding energy compared to that of the white. By subtracting the normalized Ti 2p spectra of black with white TiO_2 nanosheets, there are two extra peaks centered at ca. 462.9 and 457.7 eV (Fig. 5B).[24] These two peaks are in line with the characteristic peaks of Ti $2p_{1/2}$ and Ti $2p_{3/2}$ of Ti^{3+},[25] which confirms the presence of Ti^{3+} in the hydrogenated TiO_2 nanosheets. Fig. 5C depicts the O 1s core level XPS spectra of the different samples. After hydrogenation, a broader O 1s peak with a strong shoulder can be found at high binding energy. The shoulder peak at 531.9 eV corresponds to Ti-OH species, implying the increase of hydroxyl groups on the surfaceduring hydrogenation.[5]

Moreover, the valence band of samples displays different characteristics, as shown in Fig. 5D. The blue lines show the linear extrapolation of the curves used for deriving the band edge position. It can be found that the main absorption onset was shifted toward the vacuum level and a little tail of the maximum valence band energy appeared. All the binding energy changes during hydrogenation can be resulted from the formation of oxygen vacanciesor Ti^{3+} centers.[5] The energy band diagram was schematized (Fig. 5E) to help to understand the behavior of the black TiO_2 nanosheets. Compared with white TiO_2 nanosheets, lowering CB and tails of VB formed because of the O vacation or Ti-H bonds in the black, which are contributed to narrow the band gap of samples.[5]

In this study, photoluminescence (PL) spectra were used to characterize the oxygen vacancy and defects of samples.[26] The normalized PL spectra of different TiO_2 nanosheets at the excitation of 320 nm were shown in Fig. 5F. In all cases, a broad PL peak corresponding to the typical emission for TiO_2 can be found around 350-500 nm. After hydrogenation, the overall maximums of the emission peaks are shifted to longer wavelengths, and new peaks at 360 nm appeared and became stronger along with the increase of the hydrogenated temperature. The self-trapped excitation recombination localized at neighboring Ti^{3+}-O^- sites is considered to lead to the appearance of the new significant peaks.[6]

To investigate the improved photocatalytic performance, we explored the photoeletrochemical (PEC) behaviors of the samples. The chronoamperometry responses of black samples under illumination are obviously higher than that of the white nanosheets, as shown in Fig. 6A. And the photocurrent of sample hydrogenated at 260 ^oC reaches maximum (80 μA cm^{-2}), which is nearly four times than that of the white one. To further study the photocatalytic performance, the different

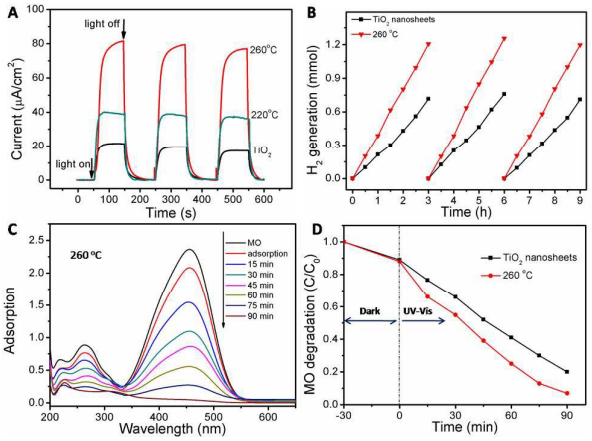

Fig. 6. (A) The chronoamperometry responses of the samples (0.6 V bais). (B) The H_2 evolution of the nanosheets. (C) The UV–vis absorption spectra of MO with black TiO_2 nanosheets (hydrogenated at 260 °C). (D) The Photocatalytic degradation of MO solution in the presence of white and black TiO_2 nanosheets.

TiO_2 nanosheets were evaluated as the H_2 evolution photocatalysts under a 300 W Xenon lamp. The black TiO_2 shows a much higher photocatalytic activity than that of the white one, its reaction rate is 400 μmol h^{-1}, while the white TiO_2 is only 263.3 μmol h^{-1}(Fig. 6B). The photodegradation of MO was chosen to test the photocatalytic activity of the as-prepared samples (AM1.5, 90 mW cm^{-2}). Fig. 6C is the UV–vis absorption spectra of MO during degradation. At first, the suspension was stirred under dark for 30 min to reach the adsorption equilibrium. In the dark stage, the samples presented an obvious adsorption of dyes because of the big specific surface area. After irradiation for 90 min, less than 6 % of the MO is kept in the suspension for the black TiO_2 nanosheets, while for the white sample, there is more than 20 % retained (Fig. 6D). The higher photocurrent response, H_2 evolution and MO degradation rate of the black TiO_2 nanosheets are all contributed to the narrow band gap and the enhancement adsorption of visible light.

In summary, we have demonstrated that black 2D TiO_2 ultrathin nanosheets can be successfully fabricated through disorder engineering on white nanosheets. TEM and XRD revealed the changes of crystal structures for the samples during the hydrogenation process. And Raman spectrum indicated that new activate mode formed as well. The changed chemical structure of the TiO_2 nanosheets from white to black is also confirmed by XPS and PL. All the characterizations indicate the unique properties of 2D TiO_2 nanosheets. Further the salient properties of black 2D TiO_2 nanosheets have been indicated that its photocurrent (80 μA cm^{-2}) is four times than that of the white one, and it presented higher solar-driven hydrogen production rate of 400 μmol h^{-1}. Therefore, the advantageous functionality of the fabricated black TiO_2 nanosheets can be expected to have wide applications from nanostructured photoelectronic devices to energy generation and storage systems.[27]

Notes and references

1 a) A. Fujishima, K. Honda, *Nature,* 1972, **238**, 37-38; b) A. Fujishima, X. Zhang, D. A. Tryk, *Surf. Sci. Rep.,* 2008, **63**, 515–582.

2 a) M. Nasrollahzadeh, *RSC Adv.*, 2014, **4**, 29089-29093; b) Y. Xie, K. Ding, Z. Liu, R. Tao, Z. Sun, H. Zhang, G. An, *J. Am. Chem. Soc.*, 2009, **131**, 6648–6649; c) R. Ajay Rakkesh, S. Balakumar, *Journal of Nanoscience and Nanotechnology*, 2013, **13**, 370-376.

3 a) J. Virkutyte, R. S. Varma, *RSC Adv.*, 2012, **2**, 1533-1539; b) S. Wang, T. Wang, W. Chen, T. Hori, *Chem. Commun.*, 2008, 3756-3758; c) K. Ding, Z. Miao, Z. Liu, Z. Zhang, B. Han, G. An, S. Miao, Y. Xie, *J. Am. Chem. Soc.*, 2007, **129**, 6362–6363; d) D. Durgalakshmi, R. Ajay Rakkesh, S. Balakumar, *Applied Surface Science*, 2015, **349**, 561–569.

4 a) J. L. Gole, J. D. Stout, C. Burda, Y. Lou, X. Chen, *J. phys. Chem. B,* 2004, **108**, 1230–1240; b) X. Wu, J. Liu, Z. Chen, Q, Yang, C. Li, G. Lu, L. Wang, *J. Mater. Chem.,* 2012, **22**, 10438–10440; c) R. Ajay Rakkesh, D. Durgalakshmi, S. Balakumar, *J. Mater. Chem. C*, 2014, **2**, 6827–6834; d) G. Sahu, S. W. Gordon, M. A. Tarr, *RSC Adv.*, 2012, **2**, 573-582; e) T. Wang, S. Wang, W. Chen, W. Wang, Z. Xu, Y. Liu, T. Hori, *J. Mater. Chem.*, 2009, **19**, 4692-4694.

5 a) X. Chen, L. Liu, Y. Y. Peter, S. S. Mao, *Science,* 2011, **331**, 746–750; b) T. Xia, P. Wallenmeyer, A. Anderson, J. Murowchick, L. Liu, X. Chen, *RSC Adv.*, 2014, **4**, 41654-41658.

6 N. Liu, V. Häublein, X. Zhou, U. Venkatesan, M. Hartmann, M. Mačković, P. Schmuki, *Nano letters,* 2015, **15**, 6815–6820;

7 a) A. Naldoni, M. Allieta, S. Santangelo, M. Marelli, F. Fabbri, S. Cappelli, V. Dal Santo, *J. Am. Chem. Soc.,* 2012, **134**, 7600–7603; b) Z. Wang, C. Yang, T. Lin, H. Yin, P. Chen, D. Wan, M. Jiang, *Adv. Funct. Mater.,* 2013, **23**, 5444–5450; c) M. M. Khan, S. A. Ansari, D. Pradhan, M. O. Ansari, D. H. Han, J. Lee, M. H. Cho, *J. Mater. Chem. A,* 2014, **2**, 637–644.

8 Y. Wang, C. Sun, X. Yan, F. Xiu, L. Wang, S. C. Smith, K. L. Wang, G. Lu, J. Zou, *J. Am. Chem. Soc.,* 2011, **133**, 695–697.

9 Z. Sun, T. Liao, Y. Dou, S. M. Hwang, M. S. Park, L. Jiang, S. X. Dou, *Nat. commun.,* 2014, **5**, 3813.

10 S. Wendt, P. T. Sprunger, E. Lira, G. K. H. Madsen, Z. Li, J. Ø. Hansen, J. Matthiesen, A. Blekinge-Rasmussen, E. Lægsgaard, B. Hammer, F. Besenbacher, *Science,* 2008, **320**, 1755–1759.

11 P. O. Lowdin, *J. Chem. Phys.,* 1950, **18**, 365–375.

12 P. C. P. de Andrade, *Int. J. Quantum Chem.,* 2012, **112**, 3325–3332.

13 H. Tan, Z. Zhao, M. Niu, C. Mao, D. Cao, D. Cheng, P. Feng, Z. Sun, *Nanoscale,* 2014, **6**, 10216–10223.

14 T. Lin, C. Yang, Z. Wang, H. Yin, X. Lv, F. Huang, J. Lin, X. Xie, M, Jiang, *Energy Environ. Sci.,* 2014, **7**, 967–972.

15 J. Xie, H. Zhang, S. Li, R. Wang, X. Sun, M. Zhou, J. Zhou, X. W. Lou, Y. Xie, *Adv. Mater.,* 2013, **25**, 5807–5813.

16 a) G. Xiang, T. Li, J. Zhuang, X. Wang, *Chem. Commun.*, 2010, **46**, 6801–6803; b) X. Chen, L. Liu, Z. Liu, M. Marcus, W. Wang, N. A. Oyler, M. Grass, B. Mao, P. Glans, P. Yu, J. Guo, S. Mao, *Sci. Rep.,* 2013, **3**, 1510.

17 B. Erdem, R. A. Hunsicker, G. W. Simmons, E. D. Sudol, V. L. Dimonie, M. S. El-Aasser, *Langmuir,* 2001, **17**, 2664–2669.

18 a) W. Zhang, Y. He, M. Zhang, Z. Yin, Q. Chen, *J. Phys. D: Appl. Phys.,* 2000, **33**, 912; b) G. A. Tompsett, G. A. Bowmaker, R. P. Cooney, J. B. Metson, K. A. Rodgers, J. M. Seakins, *J. Raman Spectrosc.,* 1995, **26**, 57–62.

19 W. D. Zhu, C. W. Wang, J. B. Chen, D. S. Li, F. Zhou, H. L. Zhang, *Nanotechnology,* 2012, **23**, 455204.

20 a) M. A. Butler, *J. Appl. Phys.,* 1977, **48**, 1914; b) W. Zhao , W. Ma, C. Chen, J. Zhao, Z. Shuai, *J. Am. Chem. Soc.,* 2004, **126** , 4782.

21 M. Gothelid, S. Yu, S. Ahmadi, C. H. Sun, M. Zuleta, *Inter. J. Photoenergy,* 2011, **110**, 401356.

22 T. Kubo, K. Sayama, H. Nozoye, *J. Am. Chem. Soc.,* 2006, **128**, 4074-4078.

23 M. S. Lazarus, T. K. Sham, *Chem. Phys. Lett.,* 1982, **92**, 670−674.
24 X. Lu, G. Wang, T. Zhai, M. Yu, J. Gan, Y. Tong, Y. Li, *Nano letters,* 2012, **12**, 1690–1696.
25 E. McCafferty, J. P. Wightman, *Surf. Interface Anal.,* 1998, **26**, 549–564.
26 H. Yoo, M. Kim, C. Bae, S. Lee, H. Kim, T. K. Ahn, H. Shi, *J. Phys. Chem. C,* 2014, **118**, 9726–9732.
27 a) F. D. Angelis, C. D. Valentin, S. Fantacci, A. Vittadini, A. Selloni, *Chem. Rev.,* 2014, **114**, 9708–9753; b) L. Liu, X. Chen, *Chem. Rev.,* 2014, **114**, 9890−9918; c) M. Sakar, S. Balakumar, P. Saravanan, S. Bharathkumar, *Nanoscale*, 2015, **7**, 10667–10679; d) R. Ajay Rakkesh, D. Durgalakshmi, S. Balakumar, *RSC Adv.*, 2015, **5**, 18633-18641.

Graphical Abstract: